White Rose Research Online

eprints@whiterose.ac.uk
https://eprints.whiterose.ac.uk
Universities of Leeds, Sheffield and York

Deposited via The University of Sheffield.

White Rose Research Online URL for this paper:
https://eprints.whiterose.ac.uk/id/eprint/246991/

Version: Accepted Version

Article:
Wootton, M. and Brown, S. (Accepted: 2026) Petri-Net Safety Assessment of a BESS for Electrified Shipping. Ocean Engineering. ISSN: 0029-8018 (In Press)

Reuse
Items deposited in White Rose Research Online are protected by copyright, with all rights reserved unless indicated otherwise. They may be downloaded and/or printed for private study, or other acts as permitted by national copyright laws. The publisher or other rights holders may allow further reproduction and re-use of the full text version. This is indicated by the licence information on the White Rose Research Online record for the item.

Takedown
If you consider content in White Rose Research Online to be in breach of UK law, please notify us by emailing eprints@whiterose.ac.uk including the URL of the record and the reason for the withdrawal request.

UNIVERSITY OF LEEDS
University of Sheffield
UNIVERSITY of York

Petri-Net Safety Assessment of a BESS for Electrified Shipping

Mark James Wootton[a,b] and Solomon F. Brown[a,b *]

[a]School of Chemical, Materials, and Biological Engineering, The University of Sheffield, Pam Liversidge Building, Mappin Street, S1 3JD, United Kingdom
[b]The Faraday Institution, Quad One, Harwell Science and Innovation Campus, Didcot, OX11 0RA, United Kingdom
[*]Corresponding Author. *Email*: s.f.brown@sheffield.ac.uk

5th October 2026

Abstract

Electrification in the maritime sector is becoming steadily more common as part of global general decarbonisation efforts, with over 1300 vessels now utilising either hybrid or fully electric propulsion. Having already increased more than tenfold in the last decade, the number of shipborne battery energy-storage systems deployed is foreseeably set to continue growing. Presently, rechargeable lithium-ion cells predominate among installations which require appropriate management to avoid the risk of thermal runaway. Thus, it is important that applicable and useful methodologies are available to ascertain the key confluences of hazards that can threaten crew wellbeing, damage property, and impact public confidence, given the small but notable documented history of incidents. This paper develops a fundamental Petri-net approach to studying the risk assessment of such systems, using a constructed case study containing features representative of electrified seagoing vessels. The modelling yields both the system components most commonly in a failure state during an emergency and their sensitivity to operational parameters when subject to variation. Specifically, coolant circulation was most probable to have failed in a crisis event, and the greatest impact was observed with the competence of the crew with respect to their ability to identify on-board faults.

Keywords: energy storage | battery safety | maritime EV deployment | lithium-ion batteries | thermal runaway | Petri nets | risk modelling

1 Introduction

As of the mid-2020s, the world's oceans host in excess of 60 thousand merchant vessels [2], the vast majority of which rely solely on fossil fuels for their propulsion. Viable alternatives are available, however, and the proportion of full-electric and hybrid systems is expected to grow substantially [3, 4], as seen in recent trends illustrated in Figure 1. Following the ambitions set in 2018 by the International Maritime Organisation to reduce emissions of carbon dioxide and general greenhouse gases in the sector to 30% and 50% of their 2008 level by 2050, respectively [5], the rollout of electrification seems set to continue. This requires deployment of shipborne energy-storage systems for which lithium-ion batteries (LIBs) are the current frontrunner among available technologies. LIBs are not without their own hazards and must be handled appropriately to mitigate the risks associated with failure scenarios, most notably thermal runaway, *i.e.* the self-exacerbating exothermic decomposition of the chemical constituents of the battery system, generally initiated when internal temperatures reach around 400 K [6], producing hot, flammable, and toxic effluents in both gaseous and particulate form [7, 8]. Presently, the rollout of electrification is modest in proportion to total global shipping [9], but as identified by Bugryniec *et al.* [4], there is both ample historical precedent of dangerous marine LIB incidents

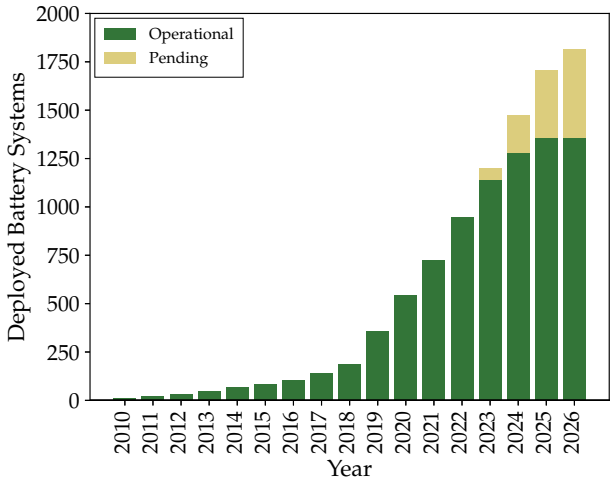


Figure 1: Operational and planned deployment of battery systems in maritime propulsion [1]

and a sufficiently large set of possible initiating events to motivate the study of safety stressors with the aim of informing best practice before the technology becomes more widespread within the sector.

The basic failure modes of a battery energy-storage system (BESS) aboard a ship will stem from a variety of internal and external factors, whose occurrence may provide the heat to initiate thermal runaway. To avert this, measures will be in place, such as a battery management system (BMS), monitoring sensors, and crew interventions. Petri nets [10], as discussed in more detail in Section 2, are well suited to assessing the failure profile of this type of system, being able to model the occurrence and confluence of any number of coincident initiating events, such as is achieved by a fault tree [11], but with complete freedom to represent non-constant failure rates, and likewise capable of modelling branching pathways within a simulated scenario, as featured in an event tree [12]. Furthermore, the methodology facilitates the seamless representation of arbitrarily complex processes of maintenance and repair, which non-simulated alternatives, such as the aforementioned, generally struggle to capture.

This work seeks to contribute to the understanding of the risks associated with maritime LIB deployment by,

- developing a fundamental Petri net modelling methodology, applied by combining component level failures and a range of real-time human interventions into a single cohesive simulation of a case-study system

  and

- utilising the model, parameterised according to data in available literature, to produce insights for the overall safety of the case study presented and for electrified shipping more generally.

2 Methodology

Since their origin, as presented in the 1962 PhD thesis of C. A. Petri [10], a number of variations extending the Petri-net methodology have been developed. The particular formalism employed in this work, defined in additional detail in Appendix A, is generalised stochastic timed atomic-fired Petri nets [10, 13, 14], *i.e.* described by,

- an expanded set of utilisable objects, *e.g.* the inhibit arc,
- possession of a simulation clock, *i.e.* events in the simulation occur at a specific time,
- containing probabilistic elements dependent on only the current marking of the system,

  and

- the selection of a single unique event at each step of simulation.

The stochastic nature of these Petri nets means that they must be sampled repeatedly by time integration so that results may be extracted in the form of simulated statistics. Although readily tractable with modern computational resources available, this is an acknowledged disadvantage by comparison to simpler methodologies. The Petri net modelling in this work is realised using the open-source software package *Macchiato* [15].

3 Case Study

For this work, a case study is constructed to demonstrate the methodology with a non-exhaustive range of generic features reasonably typical of contemporary/near-future marine-EV deployment using LIB technology, agnostic to any of the specific chemical variations. The failure modes are based on hazards identified by Bugryniec *et al.* [4], with the system illustrated

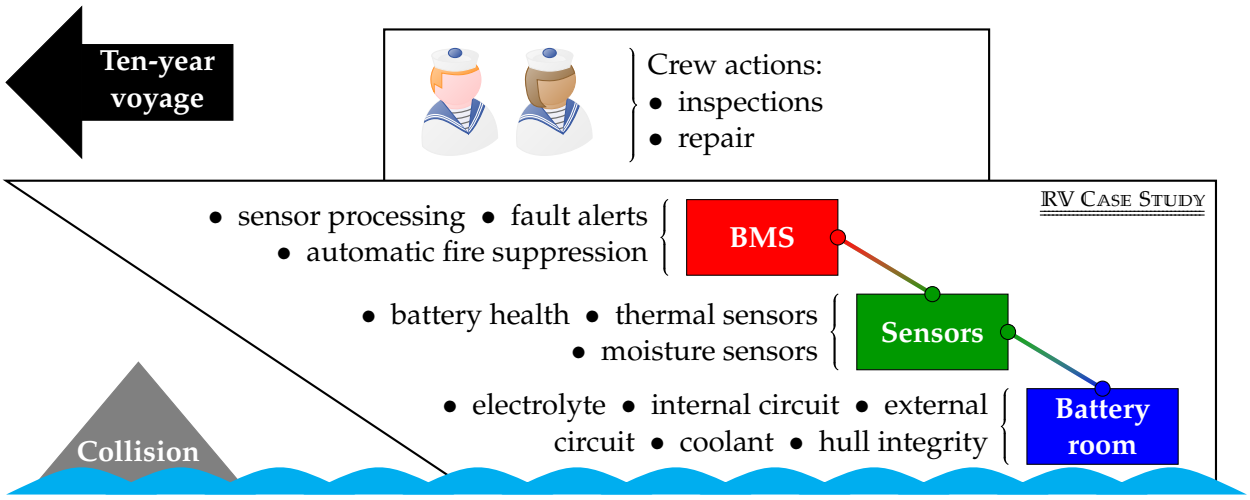


Figure 2: Schematic of the shipborne battery energy-storage system case study modelled in this work

in Figure 2. The vessel operates for a period of ten years, leading to one of two outcomes: the completion of its voyage without incident or the development of a scenario requiring emergency action to contain or avert thermal runaway in the BESS, in excess of normal maintenance and repair. The features of the system considered consist of a range of basic failures, automated processes, and the crew-executed actions of inspection and repair. Failure modes are divided into those directly affecting the battery and its housing, resulting in the production of heat and leading to thermal runaway if unchecked, and faults in the BMS and its sensors, preventing automated alerts from being issued to the crew or the activation of response systems such as automated fire suppression. All failure modes may arise spontaneously or be triggered following a collision between the ship and any manner of obstacle, be that another vessel, debris, or natural phenomena. As well as any other failure modes not explicitly referenced, possibilities not considered as part of this study include fires or faults unrelated to the BESS or wildcard external events, such as piracy or military conflict. Similarly, no regard is given to the particular location within the course of voyage undertaken by a vessel, although this would be a consideration for the risk assessment specific to a given real-world instance.

The BESS itself may suffer leakage of the battery electrolyte, internal short circuit due to issues such as dendritic growth [16], external short circuit due to issues regarding the electrical cables exterior to the battery itself within its housing space, loss of pressure in the coolant system required for a BESS of such a scale, and compromised hull integrity leading to the ingress of seawater to the battery space. The coolant failure is considered distinct from the short-circuit modes as it is assumed that the recommendations of Bugryniec *et al.* [4], *i.e.* to adopt best practice from the automotive-EV sector by employing a dielectric fluid [17], are followed. Thus, in the event of inadequate coolant circulation, the heat source applying stress to the battery is its own thermal waste emission which would otherwise be safely advected away.

The sensors and BMS monitor the BESS for anomalies of temperature, moisture, and electrical behaviour. Any detection of high temperature, water ingress, low coolant pressure, or an external short circuit sends direct alerts to the crew for further scrutiny. As internal short circuits and electrolyte leaks require maintenance beyond what is practical to action mid-voyage, detection of these faults escalates to emergency action in pre-emption of thermal runaway. Failure of monitoring and control features can delay crew awareness of problems sufficiently ahead of time to avoid this outcome.

The crew perform periodic inspection of accessible components, namely the external electrical cables, the coolant circulation, the integrity of the hull against water ingress, the thermal sensors, and the moisture sensors, with repair undertaken if faults are successfully identified, with additional inspections taken in the immediate aftermath of a collision. Likewise, repairs are effected in response to warning raised by the BMS or sensors. The capacity of the crew to contain emerging situations is finite, such that there is a non-trivial probability of their

failure to recognise failure modes. Furthermore, once aware of repairable issues, only a limited number of teams are available to perform the tasks. Repairs vary in duration as some specific incidents may prove more challenging than others, but it is assumed that given enough time, any of the accessible failure modes will be tractable, with the availability of spare parts not considered within the scope of this work.

Probabilities and parameters for the system are presented with the model itself in Section 4 after the Petri-net methodology is discussed.

4 Model

The structure of the Petri net featured in this work with its initial marking is seen in Figure 3, colour-coded by the function of each section, with the parameters for the default configuration located in Table 1. The corresponding encoding as an input file for Macchiato is found in Appendix B. The estimates found in the 2020 report *EMSA Maritime Battery Study – Electrical Energy Storage for Ships* for the rate of component failures in seagoing systems are taken as the basis for Weibull scale parameters with shape parameters drawn from a variety of sources [19–22]. Information is not always available at the desired level of granularity, and in some cases a broad estimate is used. This is partially compensated for later when the structure of the model is used as a basis for examining variations in parameters.

Throughout the description of the model, the asterisk symbol, "*", is used as a wildcard to indicate all objects whose label matches the surrounding text, with the asterisk corresponding to any string of characters. For example, `T_*_Repair` would capture repair processes, `T_A_Repair`, `T_B_Repair`, and `T_C_Repair`, but not inspection processes, `T_A_Inspc`, `T_B_Inspc`, or `T_C_Inspc`.

4.1 Default Configuration

Basic spontaneous failures are generated by `T_Elec_Leak`, `T_Internal_Short`, `T_External_Short`, `T_Coolant_Fault`, and `T_Water_Ingress` for the BESS components and `T_BMS_Fault`, `T_TS_Fail`, and `T_MS_Fail` for the BMS and sensors. Each of these removes a token from a place corresponding to the normal working state and marks an otherwise empty place to indicate the failed condition, setting the consequences in motion. Collisions are generated at a constant rate (*i.e.* $\beta = 1$) by `T_Collision`, which takes the token from `P_Obstacles` and adds one to `P_Alarm_Inspc` to prompt a precautionary inspection, and eight to `P_Collision_Damage`, *i.e.* one for each of the five BESS- and three BMS/sensor-failure modes. These correspond to pairs of fixed-delay and uniform transitions that generate the extent of the damage caused in terms of which failure modes are triggered, with the adjacent `P_*_lock` places ensuring that only one result for each mode can occur. When all of these places hold a token, `T_Collision_Over` fires to remove them and re-enable `T_Collision` by returning a token to `P_Obstacles`. All BESS failure modes add a token to `P_Heat_Generation` enabling the countdown to thermal runaway with a log-normal duration modelled by `T_Thermal_Runaway`. This begins immediately for all cases except a coolant fault, as waste heat from the BESS takes at least six hours of accumulation to present a critical thermal stress [18]. This is represented in the model by `T_CF_Heat` and during this grace period the crew have the opportunity to correct the problem. The direct detection of electrolyte leakage and short circuits is modelled with `T_EL_Alarm`, `T_IS_Alarm`, and `T_ES_Alarm`. As the former two are not repairable at sea, they immediately signal for an escalated response outcome by adding a token to `P_Emergency_Action`, with this response blocked by inhibit arcs from `P_BMS_Fault` if the BMS is unavailable. The latter, on the other hand, is within scope of crew-tractable maintenance and request for such action is made with the addition of a token to `P_ES_Repair`.

Detection of low coolant pressure or the ingress of water is handled by `T_CF_Alarm` and `T_WI_Alarm` respectively, providing that no token is present at `P_BMS_Fault` for the former or at `P_MS_Failed` for the latter, with these transitions initiating signals prompting the crew to enact repairs. Finally, if heat generation resulting from any possible cause is detected, represented by `T_Heat_Alarm`, an inspection of all accessible components is actioned. However, in the event that the thermal sensors are not in good working order, marked by a token at `P_TS_Failed`, no such order can be received. The `P_*_lock` places below each of the sensor-activation transitions prevent them from firing more than once when stimulated.

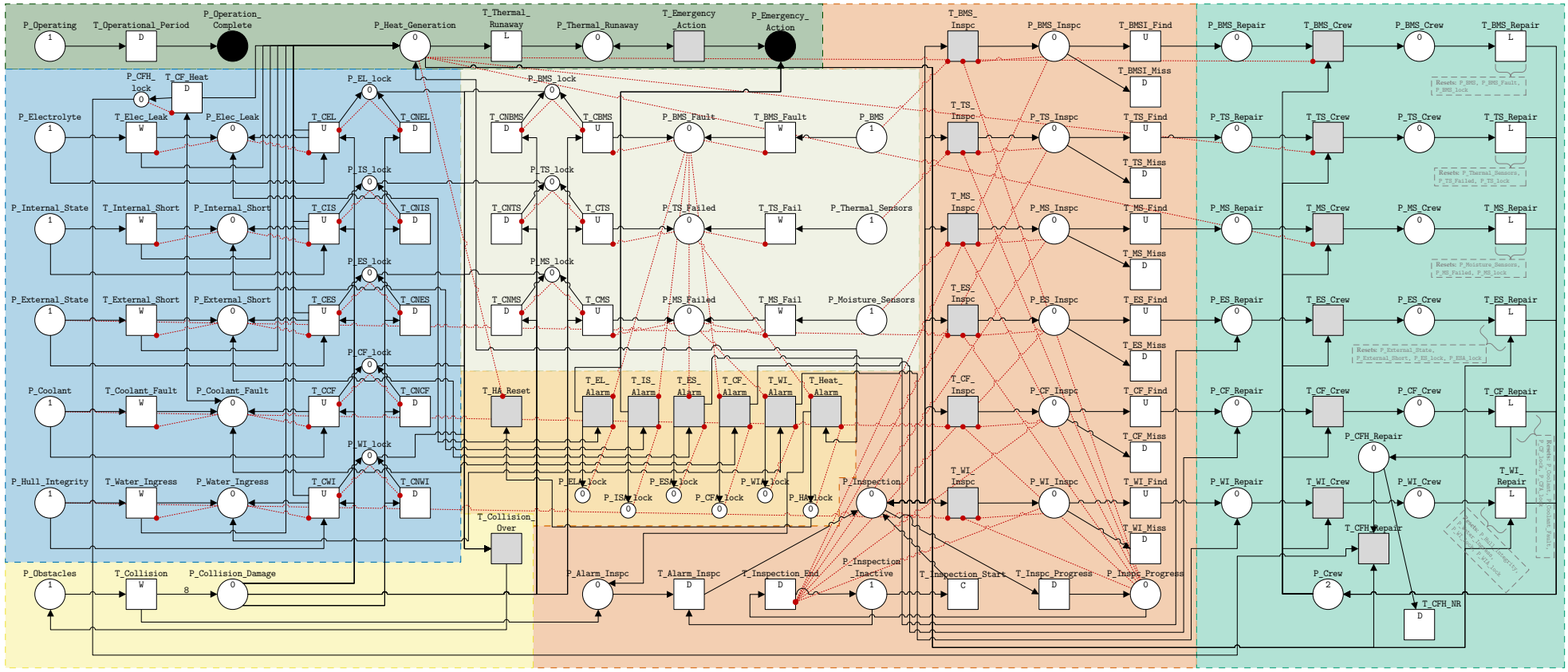


Figure 3: Petri net for the marine-EV system with initial token marking shown in default configuration. Transition parameters are found in Table 1.
Section key: terminating conditions, battery-space failure modes, monitoring failure modes, monitoring logic, collisions, inspection, repair.
Timing key: [D] fixed delay, [U] uniform distribution, [C] cyclic, [W] Weibull distribution, [L] log-normal distribution.
Places key: ○ standard, ● terminal.
Arcs: → standard, ···● inhibit, ↔ test.

This figure is available separately as a scalable vector image at: `https://doi.org/10.6084/m9.figshare.33973177`.

Table 1: Transition timing parameters for the Petri net seen in Figure 3. Approximate mean failure times are taken from estimates found in *EMSA Maritime Battery Study – Electrical Energy Storage for Ships* [18] with shape parameters set based on refs. [19–22]. Given that human error is a major risk factor for incidents [23], a pessimistic estimate is used for crew fault-recognition probability. Where no data is available, a reasonable best estimate is inserted. The symbol, $*$, is used as a catch-all to indicate all transitions with the rest of the given label in common. Parameter labels correspond to the relevant probability density function from Appendix A.iv. See equations (A.7) and (A.10) for the relationships between the Weibull and log-normal distributions and their respective means and medians. The function of each transition within the Petri net and its role in representing the mechanisms of the case-study system is described in further detail in Section 4.1.

Event	Transition	Type	Parameters	Ref.	Event	Transition	Type	Parameters	Ref.
Operational period	`T_Operational_Period`	delay	a=87660 hrs	$^N/_A$	Moisture sensor failure ($\bar{x}$=10 years)	`T_MS_Fail`	Weibull	η=94914 hrs, β=1.3	[18, 22]
Inspection period	`T_Inspection_Start`	cyclic	c=8766.0 hrs ω=0.0000 hrs	$^N/_A$	Collision with obstacle ($\bar{x}$=100 years)	`T_Collision`	Weibull	η=8.7660$\times10^5$ hrs, β=1	[18]
Inspection complete	`T_Inspection_End`	delay (nominal)	a=0 hrs	$^N/_A$	Collision electrolyte leak ($\mathbb{P}$=11%)	`T_CEL`	uniform	u=2.5000$\times10^{-3}$ hrs	$^N/_A$
Inspection in progress	`T_Inspc_Progress`	delay (nominal)	a=0 hrs	$^N/_A$	No collision electrolyte leak	`T_CNEL`	delay	a=2.7778$\times10^{-4}$ hrs	$^N/_A$
Inspection alarm call from fault	`T_Alarm_Inspc`	delay (nominal)	a=3.0000$\times10^{-4}$ hrs	$^N/_A$	Collision internal short ($\mathbb{P}$=11%)	`T_CIS`	uniform	u=2.5000$\times10^{-3}$ hrs	$^N/_A$
Successful detection of fault by inspection ($\mathbb{P}$=50%)	`T_*_Find`	uniform	u=5.5556$\times10^{-4}$ hrs	$^N/_A$	No collision internal short	`T_CNIS`	delay	a=2.7778$\times10^{-4}$ hrs	$^N/_A$
Unsuccessful detection of fault by inspection	`T_*_Miss`	delay	a=2.7778$\times10^{-4}$ hrs	$^N/_A$	Collision external short ($\mathbb{P}$=25%)	`T_CES`	uniform	u=1.1111$\times10^{-3}$ hrs	$^N/_A$
Repair time ($\bar{x}$=6 hrs)	`T_*_Repair`	log-normal	μ=1.6668, σ=0.5	$^N/_A$	No collision external short	`T_CNES`	delay	a=2.7778$\times10^{-4}$ hrs	$^N/_A$
Time from coolant failure to critical heat accumulation	`T_CF_Heat`	delay	a=6.0000 hrs	[18]	Collision coolant fault ($\mathbb{P}$=25%)	`T_CCF`	uniform	u=1.1111$\times10^{-3}$ hrs	$^N/_A$
Coolant fault repaired before heat generation	`T_CFH_NR`	delay (nominal)	a=0 hrs	$^N/_A$	No collision coolant fault	`T_CNCF`	delay	a=2.7778$\times10^{-4}$ hrs	$^N/_A$
Progression from heat generation to thermal runaway ($\tilde{x}$=8 hrs)	`T_Thermal_Runaway`	log-normal	μ=2.0794, σ=1.0000	$^N/_A$	Collision water ingress ($\mathbb{P}$=50%)	`T_CWI`	uniform	u=5.5556$\times10^{-4}$ hrs	$^N/_A$
Electrolyte leak ($\bar{x}$=100 years)	`T_Elec_Leak`	Weibull	η=9.7427$\times10^5$ hrs, β=3.50000	[18, 19]	No collision water ingress	`T_CNWI`	delay	a=2.7778$\times10^{-4}$ hrs	$^N/_A$
Internal short ($\bar{x}$=100 years)	`T_Internal_Short`	Weibull	η=9.7427$\times10^5$ hrs, β=3.5000	[18, 19]	Collision BMS fault ($\mathbb{P}$=11%)	`T_CBMS`	uniform	u=2.5000$\times10^{-3}$ hrs	$^N/_A$
External short ($\bar{x}$=100 years)	`T_External_Short`	Weibull	η=9.8573$\times10^5$ hrs, β=1.8000	[18, 20]	No collision BMS fault	`T_CNBMS`	delay	a=2.7778$\times10^{-4}$ hrs	$^N/_A$
Coolant fault ($\bar{x}$=1 year)	`T_Coolant_Fault`	Weibull	η=9.3190$\times10^3$ hrs, β=1.2000	[18, 21]	Collision thermal sensor failure ($\mathbb{P}$=11%)	`T_CTS`	uniform	u=2.5000$\times10^{-3}$ hrs	$^N/_A$
Water ingress ($\bar{x}$=10 years)	`T_Water_Ingress`	Weibull	η=9.8166$\times10^4$ hrs, β=3.0000	[18, 21]	No collision thermal sensor failure	`T_CNTS`	delay	a=2.7778$\times10^{-4}$ hrs	$^N/_A$
BMS fault ($\bar{x}$=10 years)	`T_BMS_Fault`	Weibull	η=9.4914$\times10^4$ hrs, β=1.3000	[18, 22]	Collision moisture sensors failure ($\mathbb{P}$=11%)	`T_CMS`	uniform	u=2.5000$\times10^{-3}$ hrs	$^N/_A$
Thermal sensors failure ($\bar{x}$=10 years)	`T_TS_Fail`	Weibull	η=9.4914$\times10^4$ hrs, β=1.3000	[18, 22]	No collision moisture sensor failure	`T_CNMS`	delay	a=2.7778$\times10^{-4}$ hrs	$^N/_A$

The inspection process is initiated both by any one of the aforementioned triggers and on a yearly basis. The former takes place after P_Alarm_Inspc receives a token to enable T_Alarm_Inspc, which fires after a brief delay to ensure the state of post-collision damage is fully resolved, with the latter implemented with a cyclic transition, T_Inspection_Start. Both transitions take a token from P_Inspection_Inactive and add one to P_Inspection, enabling all of the T_*_Inspc transitions if the corresponding failure mode is in effect [1], each adding a token to the relevant P_*_Inspc place on firing. This is implemented via test arcs between P_Inspection and each of T_*_Inspc, with the progression of a token through T_Inspc_Progress, P_Inspc_Progress, T_Inspection_End, back to P_Inspection_Inactive regulating the activation of the mechanism, using inhibit arcs from P_Inspc_Progress to each T_*_Inspc and from the P_*_Inspc places to the transitions T_*_Inspc and T_Inspection_End. Subsequently, when inspection is necessary, a pair of transitions T_*_Find and T_*_Miss, respectively with uniform distributions and fixed delays, simulates the successful or unsuccessful detection of each fault by the crew. Given that human error is frequently found to be the source of mishaps at sea [23], a somewhat pessimistic estimate has been chosen for the likelihood of correct identification of faults, with the probability set at 50%. Success leads to the start of a repair process, marked by a token being added to the corresponding P_*_Repair place, and failure, conversely, to no further action.

The number of teams available to work on repairs is indicated by the number of tokens at P_Crew, with two standing by if no such activities are currently in progress. When demand arrives at a P_*_Repair place, the pool of available teams is temporarily reduced by the adjacent T_*_Crew transition, which assigns them to a P_*_Crew place while the work is being carried out. They remain there for a period generated by the log-normal transitions, T_*_Repair, representing the duration of the task. On firing, these transitions return the team to the P_Crew pool, and, having a reset relation with the places corresponding to the fault and its detection, restore their token marking to indicate normal operation has resumed. The transitions T_CFH_Repair and T_CFH_NR cancel the heat-accumulation countdown specific to failed coolant circulation. As inspections carried out in the aftermath of a collision do not affect the timing of periodic inspections, it is possible for a duplicate repair to be requested if a component is damaged by an impact that occurs very close to when the next routine inspection is due, such that the repairs are still underway at that time. While this could unnecessarily occupy a crew team, the consequences for the simulation results are minimal, given that collisions occur at rate of around once per hundred years in contrast to repairs which can be completed typically in a matter of hours.

If heat generation is already in progress, repairs to the BMS and sensors cannot be undertaken, with inhibit arcs from P_Heat_Generation to each of the relevant transitions enforcing this block. Left unchecked, heat generation progresses to thermal runaway after a duration given by the transition T_Thermal_Runaway via a log-normal distribution. Reaching such a condition, denoted by a token at P_Thermal_Runaway, requires urgent intervention. Thus, the transition T_Emergency_Action fires, ending the simulation.

4.2 Sensitivity Variations

An aim of this work is to demonstrate sensitivity analysis as implemented in a Petri net. Thus, variations on the model are executed and contrasted. Three factors are considered:

- N_C the number of crew repair teams available to correct failure modes concurrently,
- T_I the period between routine inspections, and
- P_I the competence of the crew with respect to their success rate in detecting faults during inspections

with alterations simulated wherein their values are adjusted $\pm 50\%$, all other parameters being as described in the default configuration and only one factor subject to experimentation at a time. These three factors correspond respectively to the initial token count of P_Crew, the value of c for T_Inspection_Start, and the value of u for T_*_Find.

[1] Unlike in the case of a fault, it is assumed that the crew always appropriately identify a correctly functioning component, so the inspection is skipped by the model to avoid unnecessary computational expenditure.

5 Results & Discussion

Being a stochastic model, the Petri net must be repeatedly sampled to produce statistics describing its behaviour. For each configuration discussed, 10^5 iterations were conducted to yield results with sufficient statistical confidence for the purposes of this work, estimated as described in Appendix C. A statistical overview of the performance of each parameter set is given in Table 2 and time-dependent characterisations of the data are visualised from Figures 4 to 10. Results expressed as a function of time are quoted with respect to years, defined for the purposes of this work as 8766 hours, based on the approximate length of an average year in the Gregorian calendar, *i.e.* 365.25 days of 24 hours, with the term "month" referring to one twelfth of this value, *i.e.* 730.5 hours. As seen in Figure 4 and Table 2, around 40% of a population of vessels will encounter the need for emergency action before the mid-point of their voyage for all parameter variations, with the probability reaching around 70% before the end of the ten years. This very high attrition rate may indicate that the generic failure rates given in the main source for electrified shipping hazards, namely *EMSA Maritime Battery Study – Electrical Energy Storage for Ships* [18] or the estimates used for other probabilities are substantially over pessimistic (the high failure rate of the coolant system is particularly notable, as discussed later). Alternatively, if the failure rates are assumed to be reasonable, the conclusion follows that a real system which is otherwise similar in form would need to include considerable redundancy to be able to operate with any degree of acceptable safety, possibly supplemented by additional risk-management mechanisms *e.g.* a robust emergency battery shutdown mechanism to alleviate exacerbating strain when supporting components are dysfunctional, or the installation of ultrasound sensors [24] to provide a parallel means to monitor battery state of health. Regardless, it is stressed that outcomes presented in this work pertain to its hypothetical case study and not the likelihood of emergency scenarios for any extant vessel.

In Figure 5, it is seen that the risk to the system rises quickly in the first year of the voyage, followed by a relatively flat peak roughly from between two to four years, transitioning in a steady decline thereafter. The visible oscillations can be accounted for by their correspondence

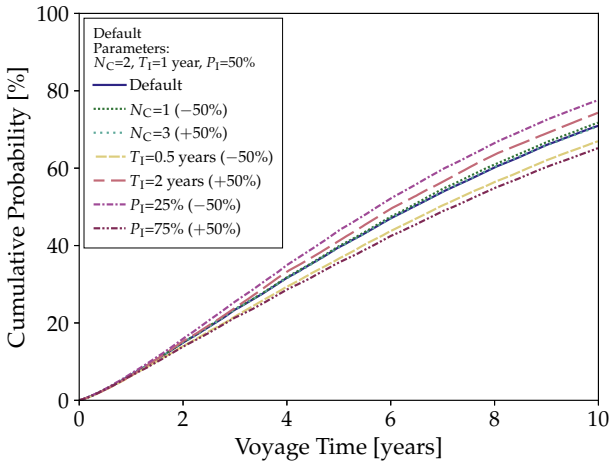


Figure 4: Cumulative probability of the requirement for emergency action resulting from variations of the system parameters is shown with respect to duration into the voyage of the marine-EV.

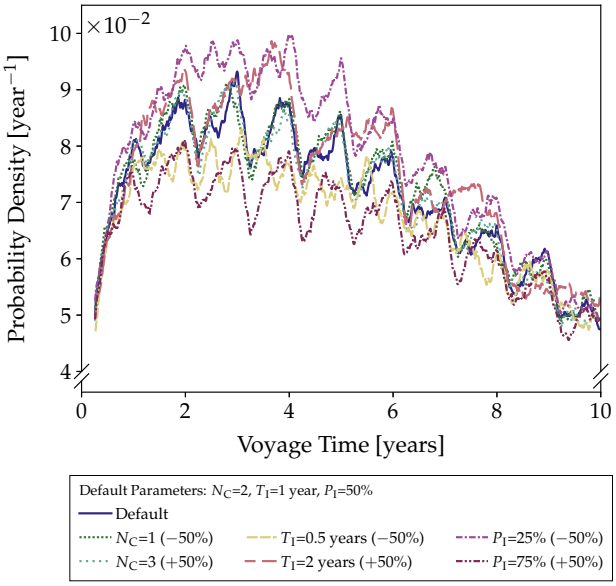


Figure 5: Estimated probability density of the marine-EV requiring emergency action with respect to time into its voyage is plotted, calculated by numerically differentiating [2] the data in Figure 4 and applying a three-month moving average to eliminate noise.

to the inspection period, with observed faults leading to escalation to emergency action.

With regard to overall impact of parameter variation, the best performance is seen by increasing the probability of correct fault identification by the crew, and conversely, an increased rate of false negatives likewise degrades outcomes. This is visible in Figure 4 by observing the relative position in each line over time and in Figure 6 where the difference in mean and median for each variation from the performance of the default parameters is

Table 2: Summary of Petri-net iterations requiring emergency action with respect to parameter variation used. The structure of the Petri net is shown in Figure 3, with default parameters in Table 1.

Parameter Variation	Mean [years]	Median [years]	Percentile		Probability within ten-year voyage [%]	Of which reaching thermal runaway [%]
			10^{th} [years]	90^{th} [years]		
Default	4.677 ± 0.010	4.496 ± 0.013	1.059 ± 0.018	8.653 ± 0.018	70.92 ± 0.14	98.26 ± 0.05
$N_C = 1$	4.683 ± 0.010	4.529 ± 0.013	1.073 ± 0.017	8.633 ± 0.017	71.75 ± 0.14	98.40 ± 0.05
$N_C = 3$	4.667 ± 0.010	4.503 ± 0.013	1.065 ± 0.018	8.615 ± 0.018	70.79 ± 0.14	98.26 ± 0.05
$T_I = 0.5$ years	4.723 ± 0.011	4.571 ± 0.013	1.053 ± 0.018	8.696 ± 0.018	66.96 ± 0.15	98.08 ± 0.05
$T_I = 2$ years	4.686 ± 0.010	4.511 ± 0.012	1.123 ± 0.017	8.619 ± 0.017	74.32 ± 0.14	98.45 ± 0.05
$P_I = 25\%$	4.638 ± 0.010	4.443 ± 0.012	1.101 ± 0.017	8.553 ± 0.017	77.56 ± 0.13	98.57 ± 0.04
$P_I = 75\%$	4.726 ± 0.011	4.586 ± 0.014	1.022 ± 0.019	8.709 ± 0.019	65.18 ± 0.15	98.04 ± 0.05

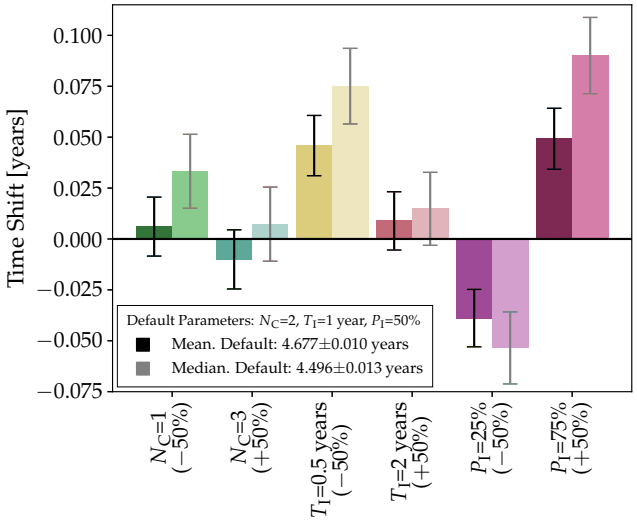


Figure 6: Impact of parameter variations on the mean and median times into the voyage at which emergency action was required for each of the parameter variations is shown with respect to the default configuration.

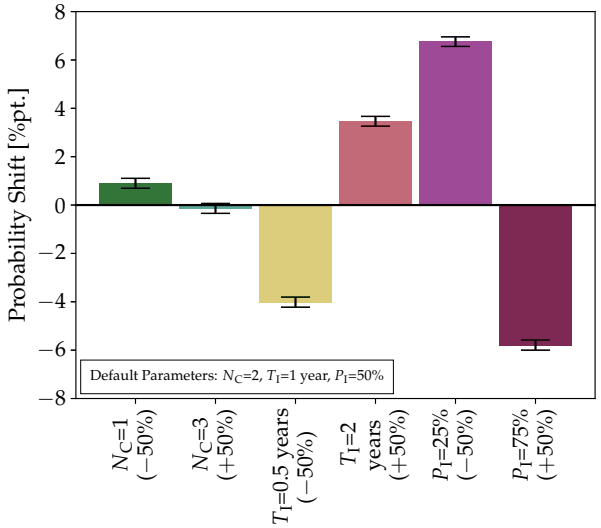


Figure 7: Impact of parameter variations on probability of thermal runaway before the end of the ten-year voyage of the marine-EV is shown with respect to the default configuration.

seen. In the latter, this impact is shown to be statistically significant and to be stronger for the case of improved crew fault recognition. However, in Figure 7, which shows the effects of each parameter change on the probability of a thermal-runaway state being reached, reduced recognition ability results in a greater increase than the decrease from enhancing it, with this parameter remaining the most impactful.

Performing inspection twice as frequently produced an improvement very close to that of the inspection success probability insofar as is seen in the small gap between their lines in Figure 4 and the visible delay in the mean and median time of emergency action in Figure 6, but in this case, a corresponding drop is not seen for this metric when inspections are conducted half as often. Nevertheless, there is a tangible impact for both variations on the probability of thermal runaway, indicating that reduced inspection frequency does in fact degrade safety, although by this measure neither increase nor decrease of the parameter in question has as great an effect as the probability of successful detection. Figure 8 shows the steady decrease in faults detected as the gap between inspection periods is increased. As fault probabilities remain the same in all cases, this implies that problems are simply being neglected at a higher rate before

[2] A central difference method is used, such that for data comprised of an n-length sequence of X_i and Y_i pairings, $(X_0, Y_0), (X_1, Y_1), (X_2, Y_2), \ldots, (X_{n-1}, Y_{n-1})$, in which

$$\forall i \in \mathbb{Z}^+, \quad X_i - X_{i-1} = X_{i+1} - X_i, \tag{1}$$

the derivative of the latter with respect to the former, Y', is approximated as

$$Y'_i \simeq \frac{Y_{i+1} - Y_{i-1}}{2(X_i - X_{i-1})}. \tag{2}$$

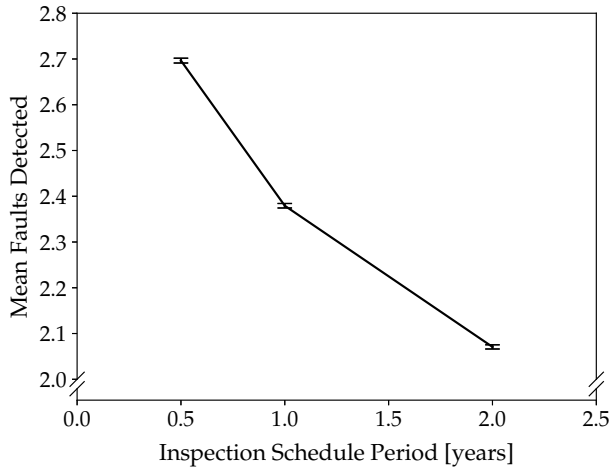


Figure 8: Mean number of faults detected by the crew over the course of the marine-EV voyage is shown with respect to the scheduled inspection period.

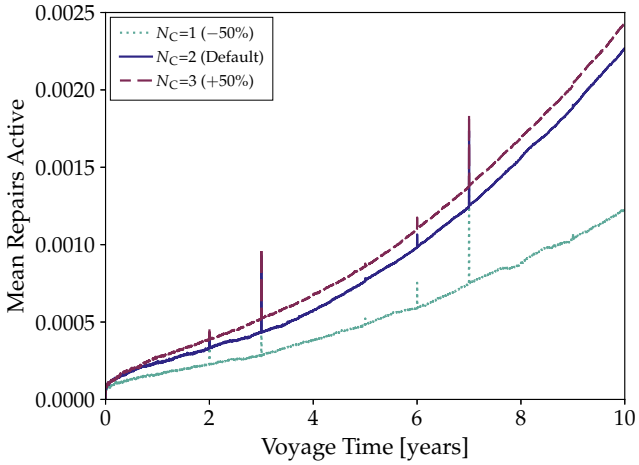


Figure 9: Mean number of crew teams engaged in repairs during the voyage of the marine-EV is shown with respect to time into its voyage.

becoming a plainly manifest problem.

The final parameter variation, *i.e.* the number of crew teams able to make simultaneous repairs, produces no statistically significant improvement when increased, but a noticeable, if small, degradation of safety when considering probability of thermal runaway as seen in Figure 7. In Figure 4, both lines are near identical over time to the default configuration, although there is a minor outlier in the median time of emergency action when only one team is present, suggesting a small increase. However, the mean time here does not show a statistically significant difference. Looking at the mean number of repairs underway with respect to time, as shown in Figure 9, it is seen that the number of component faults being worked on concurrently is substantially reduced when only one team can be engaged with these tasks, whereas the diminishing returns of additional teams are plainly visible, suggesting that the occurrence of more than two contemporaneous failures is comparatively rare. Unsurprisingly, the number of repairs in process grows over time as faults continue to manifest and spikes in activity are also observed corresponding to failures found during inspection [3].

In Figure 10, the probability of each component being in a failed state in the event of emergency action and in the event of the subset of which going into thermal runaway is illustrated, with the results for the default parameter set shown directly and all variations being displayed in terms of their deviation from its values. Despite the unique grace period, coolant faults are present in well over half of emergency action scenarios and show sensitivity to all parameter changes except the increase in repair teams, to which no component shows sensitivity, consistent with its afore-discussed minimal impact with respect to other metrics. Likely because of its grace period, coolant faults have by far the strongest sensitivity to a reduction in repair teams, with only the moisture sensors coming close to a statistically significant effect. Overall, little sensitivity is seen for the components with low initial probabilities of being in a failed state when emergency action is required, *i.e.* the electrolyte, the internal battery state, and the external state, and this should be taken as a consequence of that reduced sampling. With the exception of hull integrity, the remaining components with high probability of being in a failed state when emergency action is required, are highly sensitive to the ability of the crew to identify faults correctly and the frequency of inspections, such as to be consistent with the more general measures discussed earlier. The hull integrity does not show sensitivity to any parameter variation and this can be accounted for by its relatively high probability of being compromised during a collision event. As multiple-component damage states are most probable under such circumstances, this makes the resulting water ingress particularly likely to be represented in the system state when

[3] The state of all iterations of the Petri net for a given parameter set was sampled every 24 hours of the simulated clock, meaning the magnitude of these spikes is dependent on the confluence with the inspections. Sampling at differing intervals can shift the arrangement of spikes, but otherwise has minimal impact on the visible trends.

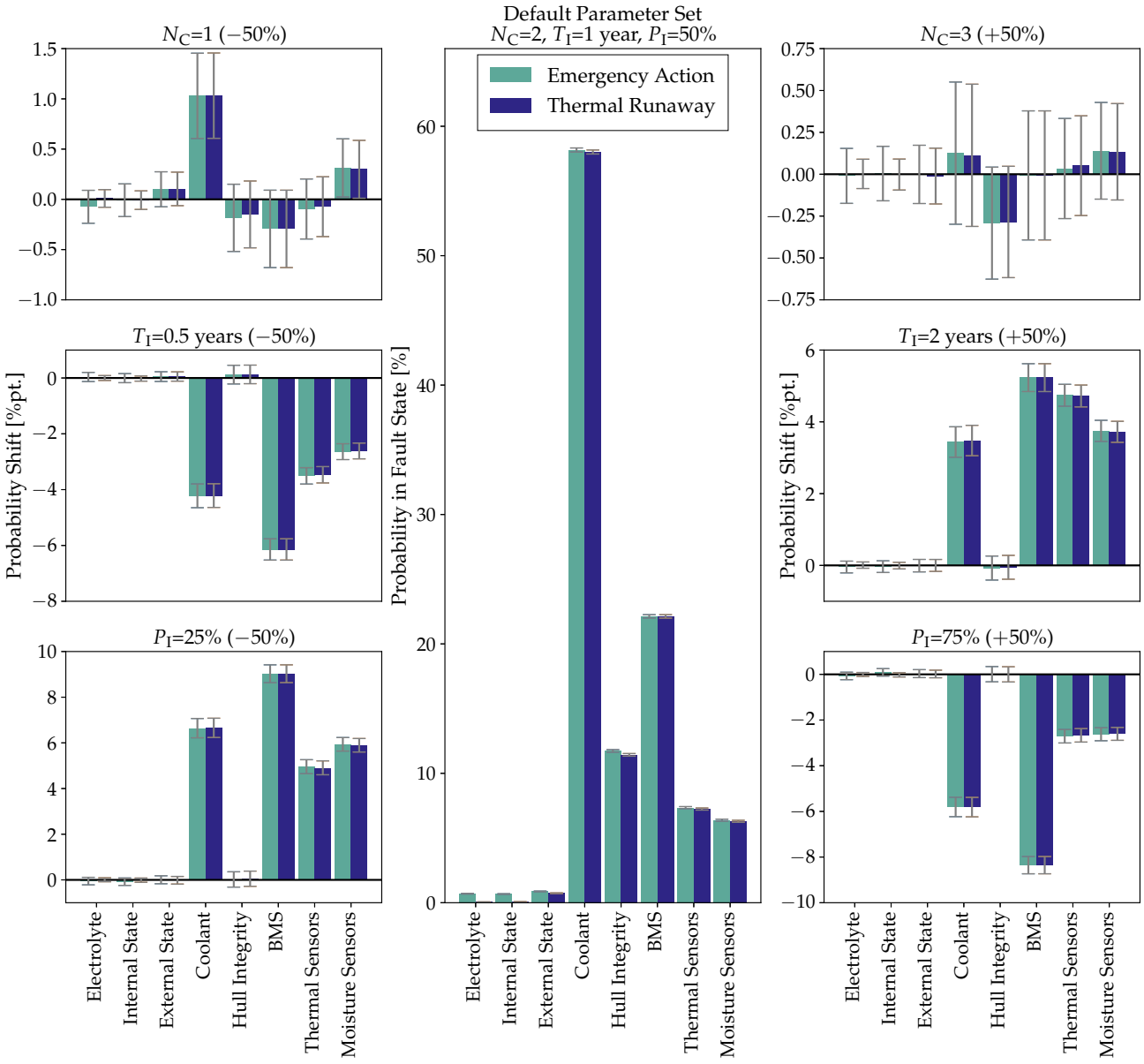


Figure 10: The central plot shows the probability that each of the components is in a failed state given that the simulation has concluded with emergency action mandated or the occurrence of thermal runaway when the default parameter configuration is used. In the surrounding plots, the percentage-point impact relative to the default configuration is plotted for each of the parameter variations studied.

a simulation-terminating crisis is reached as a result of repair resources being overwhelmed. The only factor that comes close to having a statistically significant impact is the number of repair teams present and it would be an interesting possible extension of this work to examine whether a larger volume of simulation iterations or increasing N_C to greater values than covered thus far would bear this out.

6 Conclusions

This work has developed a Petri-net-based approach for the assessment of safety considerations in electrified marine applications, using the available data in the literature to model the failure of system components and the behaviour of the crew in responding to potential crises as they develop. Having produced the initial results arising from this data, the sensitivity of the system was then examined, revealing the impact from variations on selected parameters. The model presented in this work can serve as a basis for the subsequent construction of a more verisimilitudinous case study with additional complexities and detail in the range of crew activities or with an expanded failure mode set and compound faults, derived from the specifics of either a real EV or hybrid vessel. Additionally, the failure modes considered in this work are independent and thus no consideration is given to coupled fault events, the prospect of multiple failures arising from a collision notwithstanding. Similarly, it has been assumed that if repairs are made, the relevant components can be treated as being in an "as new" state. However, it is entirely reasonable that a shorter mean time to occurrence for a failure mode may arise following the restoration of the functionality of a particular subsystem if brand-new units are not available or the same quality of work cannot be achieved mid-voyage compared to in dock. Provided the additional model complexity is considered a worthwhile trade-off for the increased fidelity, representation of both such interactions is achievable within the Petri-net framework and is a potential avenue for follow-up studies.

While these results allow one to comment in broad terms on the relative impact of the represented failure modes and parameter variations, the important takeaway is the breadth and depth of analysis that is possible with a model like this, limited only by the practical constraints of time and input data granularity to which one is subject. Certainly, if adjusting the model presented in this work to assess a real-world vessel, it would be important to take great care to consult system-specific expertise to achieve suitable parameterisation, rather than relying on the generic data available to this study. Once implemented, operators would also have the ability to experiment via simulation with changes in management strategies and operational procedures, *e.g.* as to whether some variety of human activity recognition system [25] could be used to improve crew inspection or repair performance, assuming the technological implementation was appropriate for maritime conditions. In a Petri net, this could perhaps be represented using a layer of transitions firing to model the probability that mistakes are caught by this automation following those pertaining to whether the initial action is performed correctly.

With all these possibilities for future research in mind, it is the ambition of the authors to see Petri nets added to the methodological gamut of risk and safety assessment for the ever-growing sector of battery energy-storage applications more broadly so that the spectre of hazards in the technology may be banished without compromising public confidence at this crucial transitional moment, with many other highly suitable systems available to study.

CRediT authorship contribution statement

Mark James Wootton: Conceptualisation, Methodology, Software, Visualisation, Writing – original draft. **Solomon F. Brown:** Supervision, Writing – review & editing

Orcid ID

Mark James Wootton: 0000-0001-6850-5978
Solomon F. Brown: 0000-0001-8229-8004

Declaration of competing interest

The authors declare that they have no known competing financial interests or personal relationships that could have appeared to influence the work reported in this paper.

Acknowledgements

This research was supported by the Faraday Institution [grant numbers: FIRG061 and FIRG086] as part of the *SafeBatt* project. The authors thank the fellow members of *The Brown Group* [26] for feedback during the preparation of this manuscript. Additional gratitude is expressed to the authors of the software package `matplotlib` [27, 28], used in the production of figures in this work.

References

[1] *Alternative Fuel Insights*. Tech. rep. Det Norske Veritas AS, 2026. URL: https://afi.dnv.com/statistics/DDF10E2B-B6E9-41D6-BE2F-C12BB5660105/Batteries_Vessel-Basic (visited on 17/04/2026).

[2] Statista Research Department. *Number of ships in the world merchant fleet as of January 1, 2023, by type*. 2024. URL: https://www.statista.com/statistics/264024/number-of-merchant-ships-worldwide-by-type (visited on 13/01/2025).

[3] S. Qazi, P. Venugopal, G. Rietveld, T. B. Soeiro, U. Shipurkar, A. Grasman, A. J. Watson and P. Wheeler. "Powering Maritime: Challenges and prospects in ship electrification". In: *IEEE Electrification Magazine* 11.2 (2023), pp. 74–87. ISSN: 2325-5889. DOI: 10.1109/mele.2023.3264926.

[4] P. Bugryniec, S. Khanna, M. Wootton, D. Williams and S. Brown. "Assessment of the Risks Posed by Thermal Runaway within Marine Li-Ion Battery Energy Storage Systems — Considering Past Incidents, Current Guidelines and Future Mitigation Measures". In: (2024). DOI: 10.2139/ssrn.5052235.

[5] *Initial IMO Strategy on Reduction of GHG Emissions from Ships*. Resolution MEPC.304 72/17/Add.1 Annex 11. 2018. URL: https://wwwcdn.imo.org/localresources/en/KnowledgeCentre/IndexofIMOResolutions/MEPCDocuments/MEPC.304(72).pdf.

[6] Y. Dai and A. Panahi. "Thermal runaway process in lithium-ion batteries: A review". In: *Next Energy* 6 (2025), p. 100186. ISSN: 2949-821X. DOI: 10.1016/j.nxener.2024.100186.

[7] M. Qiu, J. Liu, B. Cong and Y. Cui. "Research Progress in Thermal Runaway Vent Gas Characteristics of Li-Ion Battery". In: *Batteries* 9.8 (2023), p. 411. ISSN: 2313-0105. DOI: 10.3390/batteries9080411.

[8] Y. Yan, L. Wang, Z. Wu, J. Dong, Z. Yuan, J. Han and J. Li. "Thermal runaway and combustion of lithium-ion batteries in engine room fires on oil/electric-powered ships". In: *Applied Thermal Engineering* 254 (2024), p. 123838. ISSN: 1359-4311. DOI: 10.1016/j.applthermaleng.2024.123838.

[9] European Maritime Safety Agency. *EMSA Guidance on the Safety of Battery Energy Storage Systems (BESS) on board ships*. Version 1.0. 2023. URL: https://www.safety4sea.com/wp-content/uploads/2023/11/EMSA-Battery-Guidance_2023_11.pdf (visited on 12/01/2025).

[10] C. A. Petri. "Kommunikation mit Automaten". Language: German. PhD thesis. Technical University Darmstadt, 1962.

[11] *Fault tree analysis (FTA)*. Tech. rep. IEC 61025, Edition 2.0. International Electrotechnical Commission, 2006.

[12] M. Čepin. "Event Tree Analysis". In: *Assessment of Power System Reliability: Methods and Applications*. Springer London, 2011, pp. 89–99. ISBN: 978-0-85729-688-7. DOI: 10.1007/978-0-85729-688-7_6.

[13] W. G. Schneeweiss. *Petri Net Picture Book (An Elementary Introduction to the Best Pictorial Description of Temporal Changes)*. LiLoLe – Verlag GmbH (Publ. Co. Ltd.), 2004. ISBN: 978-3-934447-08-0.

[14] G. Balbo. "Introduction to Generalized Stochastic Petri Nets". In: *Formal Methods for Performance Evaluation – 7th International School on Formal Methods for the Design of Computer, Communication and Software Systems, SFM 2007, Bertinoro, Italy, May/June 2007, Advanced Lectures, Lecture Notes in Computer Science*. Ed. by M. Bernardo and J. Hillston. Vol. 4486.

Springer, 2007, pp. 83–131. DOI: 10.1007/978-3-540-72522-0_3.

[15] M. J. Wootton (@MJWootton-Research). GitHub repository. URL: https://github.com/MJWootton-Research/Macchiato.

[16] L. Huang, L. Liu, L. Lu, X. Feng, X. Han, W. Li, M. Zhang, D. Li, X. Liu, D. U. Sauer and M. Ouyang. "A review of the internal short circuit mechanism in lithium-ion batteries: Inducement, detection and prevention". In: *International Journal of Energy Research* 45.11 (2021), pp. 15797–15831. ISSN: 1099-114X. DOI: 10.1002/er.6920.

[17] C. Roe, X. Feng, G. White, R. Li, H. Wang, X. Rui, C. Li, F. Zhang, V. Null, M. Parkes, Y. Patel, Y. Wang, H. Wang, M. Ouyang, G. Offer and B. Wu. "Immersion cooling for lithium-ion batteries – A review". In: *Journal of Power Sources* 525 (2022), p. 231094. ISSN: 0378-7753. DOI: 10.1016/j.jpowsour.2022.231094.

[18] *EMSA Maritime Battery Study – Electrical Energy Storage for Ships*. Tech. rep. №: 2019-0217, Rev. 04, doc. №: 11B59ZDK-1. European Maritime Safety Agency, 2020. URL: https://www.emsa.europa.eu/publications/download/6186/3895/23.html (visited on 07/06/2024).

[19] S.-W. Eom, M.-K. Kim, I.-J. Kim, S.-I. Moon, Y.-K. Sun and H.-S. Kim. "Life prediction and reliability assessment of lithium secondary batteries". In: *Journal of Power Sources* 174.2 (2007), pp. 954–958. ISSN: 0378-7753. DOI: 10.1016/j.jpowsour.2007.06.208.

[20] L. Mariut and E. Helerea. "Multiple Stress Life Analysis on Underground Power Cables from Distribution Networks". In: *Technological Innovation for Value Creation*. Springer Berlin Heidelberg, 2012, pp. 275–282. ISBN: 9783642282553. DOI: 10.1007/978-3-642-28255-3_30.

[21] S. Morris. *Reliability Analytics Toolkit – Failure Rate Estimates for Mechanical Components*. 2010–2023. URL: https://www.reliabilityanalyticstoolkit.appspot.com/mechanical_reliability_data (visited on 24/03/2025).

[22] L. Wei, W. Wu and J. Xu. "Reliability Modeling of Complex Electronic System Based on Weibull Distribution". In: *Proceedings of the 2018 3rd International Conference on Modelling, Simulation and Applied Mathematics (MSAM 2018)*. msam-18. Atlantis Press, 2018. DOI: 10.2991/msam-18.2018.1.

[23] J. Sánchez-Beaskoetxea, I. Basterretxea-Iribar, I. Sotés and M. d. l. M. M. Machado. "Human error in marine accidents: Is the crew normally to blame?" In: *Maritime Transport Research* 2 (2021), p. 100016. ISSN: 2666-822X. DOI: 10.1016/j.martra.2021.100016.

[24] Y. Wu, Y. Wang, W. K. C. Yung and M. Pecht. "Ultrasonic Health Monitoring of Lithium-Ion Batteries". In: *Electronics* 8.7 (2019), p. 751. ISSN: 2079-9292. DOI: 10.3390/electronics8070751.

[25] J. Wang, X. Cai, X. Dai, M. Xia, C. Shi and W. Chen. "Multimodal Fusion-Based Human Action Recognition Using Wi-Fi CSI and Smartwatch Sensors". In: *IEEE Internet of Things Journal* 13.14 (2026), pp. 31652–31664. ISSN: 2372-2541. DOI: 10.1109/jiot.2026.3686886.

[26] *The Brown Group*. URL: https://www.browngroupsheffield.com.

[27] *Matplotlib: Visualization with Python*. URL: https://matplotlib.org.

[28] J. D. Hunter. "Matplotlib: A 2D graphics environment". In: *Computing in Science & Engineering* 9.3 (2007), pp. 90–95. DOI: 10.1109/MCSE.2007.55.

[29] A. Papoulis and S. U. Pillai. *Probability, Random Variables, and Stochastic Processes*. Ed. by C. F. Shultz and M. L. Flomenhoft. 2002, 4th ed. McGraw-Hill series in electrical and computer engineering. McGraw-Hill, 1965. ISBN: 978-0-07-122661-5.

[30] K. Murphy, C. Carter and S. Brown. "The exponential distribution: the good, the bad and the ugly. A practical guide to its implementation". In: *Annual Reliability and Maintainability Symposium. 2002 Proceedings*. Cat. №02CH37318 RAMS-02. IEEE, 2002, pp. 550–555. DOI: 10.1109/rams.2002.981701.

[31] R. Jiang and D. N. P. Murthy. "A study of Weibull shape parameter: Properties and significance". In: *Reliability Engineering & System Safety* 96.12 (2011), pp. 1619–1626. ISSN: 0951-8320. DOI: 10.1016/j.ress.2011.09.003.

[32] E. Artin. *The Gamma Function*. Trans. by M. Butler. Dover Publications, 2015. ISBN: 978-0-486-78978-1. Trans. of *Einführung in die Theorie der Gramma-Funktion*. Language: German. Hamburger Mathematische Einzelshrifen. B. G. Teubner, 1931.

[33] E. L. Crow and K. Shimizu, eds. *Lognormal Distributions, Theory and Applications*. Vol. 88. Statistics: Textbooks and Monographs. Marcel Dekker, 1988. ISBN: 978-0-8247-7803-3.

[34] G. M. Clarke and D. Cooke. *A Basic Course in Statistics*. 2004, 5th ed. John Wiley & Sons Ltd., 1978. ISBN: 978-0-470-97387-5.

[35] Y. Lu, S. Zhou, X. Zhou, S. Yang, M. Liu, X. Liu, H. Ling and Y. Lian. "A novel method of prediction for capacity and remaining useful life of lithium-ion battery based on multi-time scale Weibull accelerated failure time regression". In: *Journal of Energy Storage* 68 (2023), p. 107589. ISSN: 2352-152X. DOI: 10.1016/j.est.2023.107589.

[36] P. D. T. O'Connor and A. Kleyner. *Practical Reliability Engineering*. Wiley, 2011. ISBN: 978-1-119-96126-0. DOI: 10.1002/9781119961260.

[37] J. R. Taylor. *An Introduction to Error Analysis – The Study of Uncertainties in Physical Measurements*. 1997, 2nd ed. University Science Books, Sausalito, California, 1982. ISBN: 978-0-935702-75-0.

[38] M. B. Brown and R. A. Wolfe. "Estimation of the variance of percentile estimates". In: *Computational Statistics & Data Analysis* 1 (1983), pp. 167–174. ISSN: 0167-9473. DOI: 10.1016/0167-9473(83)90088-9.

[39] A. M. Mood, F. A. Graybill and D. C. Boes. *Introduction to the Theory of Statistics*. Ed. by B. C. Harrison and M. Eichberg. 1974, 3rd ed. Probability and Statistics. McGraw-Hill, 1950. ISBN: 0-07-042864-6.

[40] M. I. Ekum, O. Job, J. Taylor, A. Amalare, M. A. Khaleel and A. S. Ogunsanya. "Normal-power function distribution with logistic quantile function: Properties and application". In: *American Journal of Applied Mathematics and Statistics* 9.3 (2021), pp. 90–101. DOI: 10.1269/ajams-9-3-3. URL: https://pubs.sciepub.com/ajams/9/3/3/.

[41] E. F. Brayer. "Calculating the Standard Error of a Proportion". In: *Applied Statistics* 6.1 (1957), p. 67. ISSN: 0035-9254. DOI: 10.2307/2985858.

Appendix A Petri-Net Integration

A.i Petri-Net Objects

All Petri-net objects featured in this work are illustrated in Figure A.1(a). Formally, a Petri net is a directed bipartite graph consisting of objects referred to as *places* and *transitions*, drawn as circles and squares, respectively. The role of places is to hold *tokens*, with the set of token markings across the places of a Petri net constituting its state at a given step in the simulation. It is common to indicate the tokens held as black dots drawn inside the place, but for the sake of simplicity, the token counts in this work are written as numeric labels instead. Transitions determine the evolution of the markings in conjunction with the connectors linking them to the places. The links are formed by *arcs* and may run either from a place to a transition, or from a transition to a place, but never like-to-like. Directionality is described with respect to the transition, such that the former is referred to as *incoming* and the latter as *outgoing*. The arc is drawn as a line between its linked objects with a marker at either the transition- or place-end to indicate incoming and outgoing arcs respectively. Two types of arc are used in this work: *standard* arcs and *inhibit* arcs, taking the form of a solid black line with a triangular marker and a dotted red line with a circular marker respectively. Standard arcs may be incoming or outgoing, but an inhibit arc may only ever be incoming. All arcs have an associated *weight* – an integer value which parameterises the relationship established between the linked place and transition. By default, an arc has a weight of one. If it takes any other value, the arc is labelled to indicate this. An incoming arc that connects to a place with a token marking equal to or greater than its weight is said to be *satisfied*. A pair consisting of an incoming arc and an outgoing arc, where both are standard type, is collectively referred to as a *test arc* if both link to the same place and transition objects and have equal weights, drawn as a single line with a marker at both ends.

A.ii Transition Firing Rules

Every simulation step, one of the transitions of the Petri net is chosen to *fire*, updating the token marking of the places linked to it by standard arcs. A transition that is eligible to fire is said to be *enabled*, requiring that two criteria be met:

1. Each of the places connected to it by standard incoming arcs must have a token marking that is **equal to or greater than** the weight of their linking arc.

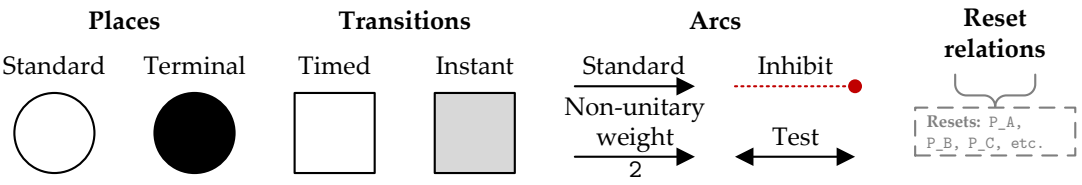
2. The token count of any place connected to the transition by an inhibit arc must be **less than** the weight of that arc.

When a transition fires, the marking of each place connected by a standard incoming arc is reduced by the weight of its connecting arc and conversely the marking of each place connected by a standard outgoing arc is increased by the weight of its connecting arc [4]. If, after firing, the conditions to enable the transition are still met, a new firing time is scheduled. Figure A.1(b–e) illustrates a Petri net in various states, with the single transition disabled in (b) and (c) due to contravention of the first and second criteria, respectively. The before and after states of the transition when enabled are shown in (d) and (e).

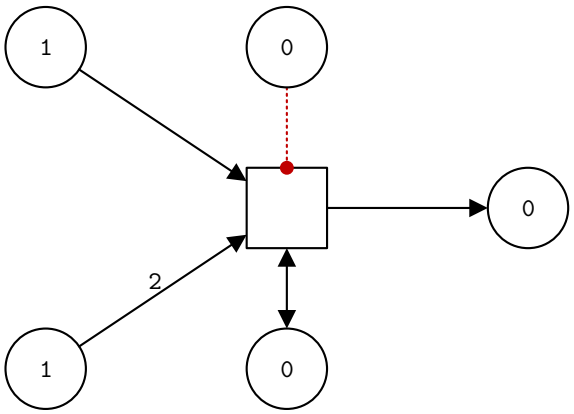
A.iii Petri-Net Time Integration

The simulation of a Petri net continues until either no transition is enabled or a place that has been designated as *terminal* receives a token. Places with this designation are coloured black, otherwise being white by default. A transition may be instant or timed, indicated by grey and white fill respectively. This determines the order in which enabled transitions are selected to fire and whether the simulated clock is advanced. When the conditions to enable a transition are first met, a time is scheduled for it to fire according to its properties. For an instant transition, firing occurs on the immediate next step, without advancement of the clock, and for a timed transition, a time is scheduled in the future. If no instant transition is enabled, the first timed transition chronologically in the schedule is selected to fire, and on doing so, the clock is updated to that time. Between first becoming

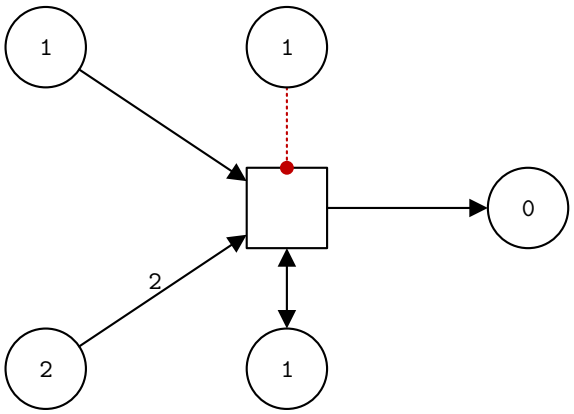
[4] Note that it is not required to conserve the number of tokens in this transaction. Except in cases specifically configured to work in such a way, thinking of tokens as being moved from one place to another should be avoided, as the tokens removed from and added to places are entirely independent.



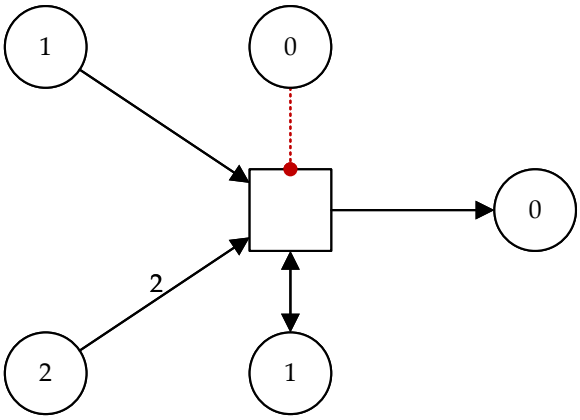
(a) Key for Petri-net objects



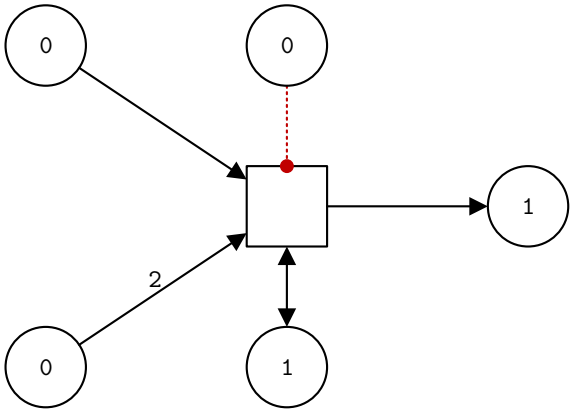
(b) The transition cannot fire because two of its three standard incoming arcs are not satisfied.



(c) Although all standard incoming arcs are satisfied, this transition is not enabled because the inhibit arc is also satisfied.



(d) All conditions for the transition to be enabled are met.



(e) The place markings have been updated with respect to the state seen in (d) following the firing of the transition. The transition is no longer enabled.

Figure A.1: (a) Constituent objects and (b – e) demonstration of transition firing rules of a Petri net including examples of standard arcs with weights of one and two, a test arc, and an inhibit arc.

enabled and firing, the enabling conditions of a transition must be met at the resolution of every intermediate step. If the conditions are interrupted for one or more steps, its enabled state is forgotten and its scheduled time to fire is discarded, calculated *de novo* if the transition is enabled again at a later step. For example, with a firing schedule, S_n, on the n^{th} step, transitions T_A, T_B, T_C, *etc.* are enabled [5] and due to fire at system-clock times as shown in equation (A.1a).

$$S_n = \begin{bmatrix} T_A : 12 \\ T_B : 13 \\ T_C : 11 \\ \vdots \; \vdots \; \vdots \end{bmatrix}. \tag{A.1a}$$

On step $n+1$, the enabling conditions for T_B are interrupted. Thus, its firing time is removed from the schedule:

$$S_{n+1} = \begin{bmatrix} T_A : 12 \\ \cancel{T_B : 13} \\ T_C : 11 \\ \vdots \; \vdots \; \vdots \end{bmatrix}. \tag{A.1b}$$

On the next step, $n+2$, T_B is enabled again, and a new time is generated, such that

$$S_{n+2} = \begin{bmatrix} T_A : 12 \\ T_B : 19 \\ T_C : 11 \\ \vdots \; \vdots \; \vdots \end{bmatrix}. \tag{A.1c}$$

In the event of multiple transitions being scheduled to fire at the same time, the conflict is resolved, first by giving priority to instant transitions, and second by selecting a transition at random if conflict remains.

A.iv Firing-Time Scheduling

Every timed transition has an associated function which determines the scheduling of its firing when it is enabled. When its transition becomes enabled, each function returns a value, x, according to a distribution, $f(x;\dots)$, which is added to the current clock to give the time scheduled for the transition to fire, *i.e.*

$$t_\text{f} = t_\text{e} + x, \tag{A.2}$$

where t_f is the system time at which the transition is scheduled to fire, provided its enabling conditions are not interrupted, having become enabled at t_e. The following schemes for generating firing times are used in this work: a fixed delay, the uniform distribution, a cyclic period, the Weibull distribution, and the log-normal distribution. A fixed-delay transition takes one parameter, $a \in \mathbb{R}^+$, which is returned for x in all cases [6], *i.e.*

$$f(x;a) = \begin{cases} 1, & x = a \\ 0, & x \neq a \end{cases}. \tag{A.3}$$

The uniform distribution also takes a single parameter, $u \in \mathbb{R}^+_*$, which sets the upper bound for returned values of x, such that its probability density function is described by

$$f(x;u) = \begin{cases} \frac{1}{u}, & x \in (0,u] \\ 0, & x \notin (0,u] \end{cases}. \tag{A.4}$$

A cyclic transition fires on the first system-clock value equal to a non-zero positive integer multiple of its first parameter, $c \in \mathbb{R}^+_*$, with its second parameter, $\omega \in (-c,c)$, providing an offset. For example, two transitions with $c=1$, $\omega=0$ and $c=1$, $\omega=0.5$ could fire at clock values of 1, 2, 3, *etc.* and 1.5, 2.5, 3.5 *etc.* respectively. Uniquely among the timing schemes detailed in this section, this results in a discrete probability density function that is dependent on t_e, such that

$$f(x;c,\omega,t_\text{e}) = \begin{cases} 1, & x = \begin{cases} c+\omega, & t_\text{e} = 0 \\ \lceil \frac{t_\text{e}}{c} \rceil c + \omega - t_\text{e}, & t_\text{e} > 0. \end{cases} \\ 0, & (x - \omega + t_\text{e}) \notin \{c, \lceil \frac{t_\text{e}}{c} \rceil c\} \end{cases} \tag{A.5}$$

The Weibull distribution [29] generalises the exponential distribution [30] to allow non-constant failure rates. It is characterised by scale and shape parameters [31], respectively η and β, where $\{\eta,\beta\} \subset \mathbb{R}^+_*$. The former broadens the spread of probability density in linear proportion to its size, with its value representing $Q(1-\exp[-1]) \simeq P_{63.2}$ of x, where $Q(\cdot)$ and $P_{(\cdot)}$ respectively denote quantile and percentile. The

[5] To avoid confusion, none of the named transitions in this example fire, with the changes to the enabling conditions of T_B caused by another unspecified transition in the elided section, avoiding the need to update the scheduled firings of T_A and T_C.

[6] It is occasionally useful to define a fixed-delay transition for which $a = 0$, creating a process that will wait for the resolution of all instant transitions before firing, without an advancement of the system clock.

latter skews the distribution either towards high early failure rates for $\beta < 1$ or rising failure rates, *i.e.* an ageing process for $\beta > 1$. The threshold $\beta = 1$ reproduces the constant failure rate of the exponential distribution. The probability density function of the Weibull distribution is given by

$$f(x;\eta,\beta) = \frac{\beta}{\eta}\left(\frac{x}{\eta}\right)^{\beta-1} \exp\left(-\left[\frac{x}{\eta}\right]^{\beta}\right), \quad \text{(A.6)}$$

which gives rise to a mean and median of

$$\bar{x} = \eta\Gamma\left(1+\beta^{-1}\right) \quad \text{and} \quad \tilde{x} = \eta\sqrt[\beta]{\ln(2)}\,, \quad \text{(A.7)}$$

in which $\Gamma(\cdot)$ is the Gamma function [32], given by

$$\Gamma(\gamma) = \int_0^\infty g^{\gamma-1}\exp(-g)\,\mathrm{d}g. \quad \text{(A.8)}$$

A log-normal distribution [33] returns a value whose natural logarithm is normally distributed [34] following a mean and standard deviation, $\mu \in \mathbb{R}$ and $\sigma \in \mathbb{R}^+_*$, respectively, resulting in a probability density function of

$$f(x;\mu,\sigma) = \frac{\exp\left(-\frac{1}{2}\left[\frac{\ln(x)-\mu}{\sigma}\right]^2\right)}{x\sigma\sqrt{2\pi}}, \quad \text{(A.9)}$$

for which the mean and median are

$$\bar{x} = \exp\left(\mu + \frac{\sigma^2}{2}\right) \quad \text{and} \quad \tilde{x} = \exp(\mu). \quad \text{(A.10)}$$

For some failure modes, this constitutes a preferable model of occurrence timing, for example LIB lifespan [35], as well as being useful in describing component-repair times where the complexity of the task is subject to variability [36].

A.v Reset Relations

A transition can also be assigned a reset relation to places not otherwise linked by arcs. When the transition fires, the token count of each of those places is restored to its initial marking, *i.e.* as it was on the zeroth step of the simulation, prior to any transitions firing. This is useful for modelling such actions as repair, where a segment of the system is entirely replaced with a fresh unit. Where applicable, the places designated in a reset relation are marked by a grey brace and label adjacent to the transition in the style illustrated in Figure A.1(a).

A.vi Branching Pathways

When two branching paths are required, *e.g.* representing the probability of correctly/incorrectly performing an action, a pair of transitions can be used to implement this process, with both having identical enabling conditions [7]. Setting parameters on an order of magnitude much smaller than characteristic of the dynamics of the system, a fixed delay and a uniform distribution can achieve the desired result. The probability of taking the upper and lower paths depicted in Figure A.2, respectively $\mathbb{P}_\uparrow$ and $\mathbb{P}_\downarrow$, is then given by

$$\mathbb{P}_\uparrow = \frac{a}{u} \quad \text{and} \quad \mathbb{P}_\downarrow = 1 - \frac{a}{u}. \quad \text{(A.11)}$$

Thus, to achieve, for example, $\mathbb{P}_\uparrow = 10\%$ and $\mathbb{P}_\downarrow = 90\%$, the two transitions should be set such that $u = 10a$, for an arbitrarily small value of a. As both transitions have their firing times entered into the schedule concurrently, in nine instances out of ten, after a nominal period of length a, the pathway stemming from the fixed-delay transition will be taken, and in the remaining one instance, the transition with the uniform distribution will fire after a delay $x \leq a$, initiating the alternative sequence.

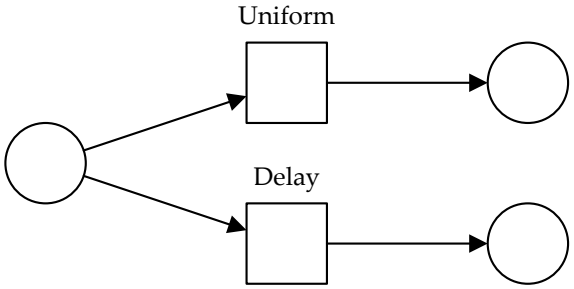


Figure A.2: In this example, a pair of transitions with uniform-distribution and fixed-delay timing schemes implement two mutually exclusive branching paths in a Petri net, using arbitrarily small parameters, u and a respectively. Their ratio determines the selection probabilities of the upper and lower outcomes in accordance with equation (A.11).

Appendix B Macchiato Code

The Petri net appearing in this work is specified below in the MPN syntax. Further details of the specification can be found in the documentation for Macchiato [15]. Please note that Weibull

[7] Conceivably, it may be desired to do otherwise to achieve a range of conditional probabilities beyond the scope of this example.

distributions are parameterised by $\bar{x}$ and β, with the appropriate η-value generated at runtime according to equation (A.7). This allows the user to change the distribution shape independently of its scale, without having to recalculate the latter manually.

```
# Petri Net Parameters
    name MarineBESS_Default
    units hrs
    runMode schedule

# Petri Net Structure
 Places
    P_Heat_Generation 0
    P_Thermal_Runaway 0
    P_Electrolyte 1
    P_Coolant 1
    P_Hull_Integrity 1
    P_Obstacles 1
    P_Internal_State 1
    P_External_State 1
    P_BMS_Fault 0
    P_BMS 1
    P_Elec_Leak 0
    P_Internal_Short 0
    P_External_Short 0
    P_Coolant_Fault 0
    P_Water_Ingress 0
    P_Collision_Damage 0
    P_Moisture_Sensors 1
    P_Thermal_Sensors 1
    P_TS_Failed 0
    P_MS_Failed 0
    P_Inspection_Inactive 1
    P_Inspection 0
    P_Emergency_Action 0
    P_IS_lock 0
    P_EL_lock 0
    P_ES_lock 0
    P_CF_lock 0
    P_WI_lock 0
    P_BMS_lock 0
    P_TS_lock 0
    P_MS_lock 0
    P_Alarm_Inspc 0
    P_ELA_lock 0
    P_ISA_lock 0
    P_ESA_lock 0
    P_CFA_lock 0
    P_WIA_lock 0
    P_HA_lock 0
    P_BMS_Inspc 0
    P_TS_Inspc 0
    P_MS_Inspc 0
    P_ES_Inspc 0
    P_CF_Inspc 0
    P_WI_Inspc 0
    P_BMS_Repair 0
    P_TS_Repair 0
    P_MS_Repair 0
    P_ES_Repair 0
    P_CF_Repair 0
    P_WI_Repair 0
    P_Inspc_Progress 0
    P_Operating 1
    P_Operation_Complete 0
    P_BMS_Crew 0
    P_TS_Crew 0
    P_MS_Crew 0
    P_ES_Crew 0
    P_CF_Crew 0
    P_WI_Crew 0
    P_Crew 2
    P_CFH_lock 0
    P_CFH_Repair 0
```

continues in single-column format:

```
Transitions
    T_Inspection_End:delay:0 IN P_Inspc_Progress:1 P_WI_Inspc:1:inh
       ↪ P_CF_Inspc:1:inh P_ES_Inspc:1:inh P_MS_Inspc:1:inh P_TS_Inspc:1:
       ↪ inh P_BMS_Inspc:1:inh OUT P_Inspection_Inactive:1
    T_MS_Crew:instant IN P_MS_Repair:1 P_Crew:1 P_Heat_Generation:1:inh
       ↪ OUT P_MS_Crew:1
    T_TS_Crew:instant IN P_TS_Repair:1 P_Crew:1 P_Heat_Generation:1:inh
       ↪ OUT P_TS_Crew:1
    T_BMS_Crew:instant IN P_BMS_Repair:1 P_Crew:1 P_Heat_Generation:1:inh
       ↪ OUT P_BMS_Crew:1
    T_BMS_Repair:lognorm:1.66676:0.5 IN P_BMS_Crew:1 OUT P_Crew:1 RESET
       ↪ P_BMS:P_BMS_Fault:P_BMS_lock
    T_WI_Inspc:instant IN P_Inspection:1 P_Inspc_Progress:1:inh
       ↪ P_Hull_Integrity:1:inh P_WI_Inspc:1:inh OUT P_Inspection:1
       ↪ P_WI_Inspc:1
    T_ES_Inspc:instant IN P_Inspection:1 P_Inspc_Progress:1:inh
       ↪ P_External_State:1:inh P_ES_Inspc:1:inh OUT P_Inspection:1
       ↪ P_ES_Inspc:1
    T_CF_Inspc:instant IN P_Inspection:1 P_Inspc_Progress:1:inh P_Coolant
       ↪ :1:inh P_CF_Inspc:1:inh OUT P_Inspection:1 P_CF_Inspc:1
```

```
T_BMS_Inspc:instant IN P_Inspection:1 P_Inspc_Progress:1:inh P_BMS:1:
    ↪ inh P_BMS_Inspc:1:inh OUT P_Inspection:1 P_BMS_Inspc:1
T_TS_Inspc:instant IN P_Inspection:1 P_Inspc_Progress:1:inh
    ↪ P_Thermal_Sensors:1:inh P_TS_Inspc:1:inh OUT P_Inspection:1
    ↪ P_TS_Inspc:1
T_MS_Inspc:instant IN P_Inspection:1 P_Inspc_Progress:1:inh
    ↪ P_Moisture_Sensors:1:inh P_MS_Inspc:1:inh OUT P_Inspection:1
    ↪ P_MS_Inspc:1
T_TS_Repair:lognorm:1.66676:0.5 IN P_TS_Crew:1 OUT P_Crew:1 RESET
    ↪ P_Thermal_Sensors:P_TS_Failed:P_TS_lock
T_MS_Repair:lognorm:1.66676:0.5 IN P_MS_Crew:1 OUT P_Crew:1 RESET
    ↪ P_Moisture_Sensors:P_MS_Failed:P_MS_lock
T_Heat_Alarm:instant IN P_Heat_Generation:1 P_TS_Failed:1:inh
    ↪ P_HA_lock:1:inh OUT P_HA_lock:1 P_Alarm_Inspc:1
    ↪ P_Heat_Generation:1
T_EL_Alarm:instant IN P_Elec_Leak:1 P_BMS_Fault:1:inh P_ELA_lock:1:inh
    ↪  OUT P_Elec_Leak:1 P_ELA_lock:1 P_Emergency_Action:1 MAX 1
T_IS_Alarm:instant IN P_Internal_Short:1 P_BMS_Fault:1:inh P_ISA_lock
    ↪ :1:inh OUT P_Internal_Short:1 P_ISA_lock:1 P_Emergency_Action:1
    ↪ MAX 1
T_ES_Alarm:instant IN P_External_Short:1 P_BMS_Fault:1:inh P_ESA_lock
    ↪ :1:inh OUT P_External_Short:1 P_ESA_lock:1 P_ES_Repair:1
T_CF_Alarm:instant IN P_Coolant_Fault:1 P_BMS_Fault:1:inh P_CFA_lock
    ↪ :1:inh OUT P_Coolant_Fault:1 P_CFA_lock:1 P_CF_Repair:1
T_WI_Alarm:instant IN P_Water_Ingress:1 P_MS_Failed:1:inh P_WIA_lock
    ↪ :1:inh OUT P_Water_Ingress:1 P_WIA_lock:1 P_WI_Repair:1
T_Thermal_Runaway:lognorm:2.07944:1 IN P_Heat_Generation:1 OUT
    ↪ P_Thermal_Runaway:1
T_BMS_Fault:weibull:87660:1.3 IN P_BMS:1 P_BMS_Fault:1:inh OUT
    ↪ P_BMS_Fault:1
T_TS_Fail:weibull:87660:1.3 IN P_Thermal_Sensors:1 P_TS_Failed:1:inh
    ↪ OUT P_TS_Failed:1
T_MS_Fail:weibull:87660:1.3 IN P_Moisture_Sensors:1 P_MS_Failed:1:inh
    ↪ OUT P_MS_Failed:1
T_Elec_Leak:weibull:876600:3.5 IN P_Electrolyte:1 P_Elec_Leak:1:inh
    ↪ OUT P_Elec_Leak:1 P_Heat_Generation:1
T_Coolant_Fault:weibull:8766:1.2 IN P_Coolant:1 P_Coolant_Fault:1:inh
    ↪ OUT P_Coolant_Fault:1
T_Water_Ingress:weibull:87660:3 IN P_Hull_Integrity:1 P_Water_Ingress
    ↪ :1:inh OUT P_Water_Ingress:1 P_Heat_Generation:1
T_Internal_Short:weibull:876600:3.5 IN P_Internal_State:1
    ↪ P_Internal_Short:1:inh OUT P_Internal_Short:1 P_Heat_Generation
    ↪ :1
T_External_Short:weibull:876600:1.8 IN P_External_State:1
    ↪ P_External_Short:1:inh OUT P_External_Short:1 P_Heat_Generation
    ↪ :1
T_CWI:uniform:0.000555556 IN P_Collision_Damage:1 P_Hull_Integrity:1
    ↪ P_WI_lock:1:inh P_Water_Ingress:1:inh OUT P_WI_lock:1
    ↪ P_Water_Ingress:1 P_Heat_Generation:1
T_CCF:uniform:0.001111111  IN P_Collision_Damage:1 P_Coolant:1
    ↪ P_CF_lock:1:inh P_Coolant_Fault:1:inh OUT P_CF_lock:1
    ↪ P_Coolant_Fault:1
T_CES:uniform:0.001111111  IN P_Collision_Damage:1 P_External_State:1
    ↪ P_ES_lock:1:inh P_External_Short:1:inh OUT P_ES_lock:1
    ↪ P_External_Short:1 P_Heat_Generation:1
T_CIS:uniform:0.0025 IN P_Collision_Damage:1 P_Internal_State:1
    ↪ P_IS_lock:1:inh P_Internal_Short:1:inh OUT P_IS_lock:1
    ↪ P_Internal_Short:1 P_Heat_Generation:1
T_CEL:uniform:0.0025 IN P_Collision_Damage:1 P_Electrolyte:1 P_EL_lock
    ↪ :1:inh P_Elec_Leak:1:inh OUT P_EL_lock:1 P_Elec_Leak:1
    ↪ P_Heat_Generation:1
```

```
T_CNWI:delay:0.000277778 IN P_Collision_Damage:1 P_WI_lock:1:inh OUT
    ↪ P_WI_lock:1
T_CNCF:delay:0.000277778 IN P_Collision_Damage:1 P_CF_lock:1:inh OUT
    ↪ P_CF_lock:1
T_CNES:delay:0.000277778 IN P_Collision_Damage:1 P_ES_lock:1:inh OUT
    ↪ P_ES_lock:1
T_CNIS:delay:0.000277778 IN P_Collision_Damage:1 P_IS_lock:1:inh OUT
    ↪ P_IS_lock:1
T_CNEL:delay:0.000277778 IN P_Collision_Damage:1 P_EL_lock:1:inh OUT
    ↪ P_EL_lock:1
T_CBMS:uniform:0.0025 IN P_Collision_Damage:1 P_BMS_lock:1:inh
    ↪ P_BMS_Fault:1:inh OUT P_BMS_lock:1 P_BMS_Fault:1
T_CNBMS:delay:0.000277778 IN P_Collision_Damage:1 P_BMS_lock:1:inh OUT
    ↪  P_BMS_lock:1
T_CTS:uniform:0.0025 IN P_Collision_Damage:1 P_TS_lock:1:inh
    ↪ P_TS_Failed:1:inh OUT P_TS_lock:1 P_TS_Failed:1
T_CNTS:delay:0.000277778 IN P_Collision_Damage:1 P_TS_lock:1:inh OUT
    ↪ P_TS_lock:1
T_CMS:uniform:0.0025 IN P_Collision_Damage:1 P_MS_lock:1:inh
    ↪ P_MS_Failed:1:inh OUT P_MS_lock:1 P_MS_Failed:1
T_CNMS:delay:0.000277778 IN P_Collision_Damage:1 P_MS_lock:1:inh OUT
    ↪ P_MS_lock:1
T_Collision:weibull:876600:1 IN P_Obstacles:1 OUT P_Collision_Damage:8
    ↪  P_Alarm_Inspc:1
T_Inspection_Start:cyclic:8766:0 IN P_Inspection_Inactive:1 OUT
    ↪ P_Inspection:1
T_BMSI_Find:uniform:0.000555556  IN P_BMS_Inspc:1 OUT P_BMS_Repair:1
T_BMSI_Miss:delay:0.000277778 IN P_BMS_Inspc:1 OUT
T_TS_Find:uniform:0.000555556  IN P_TS_Inspc:1 OUT P_TS_Repair:1
T_TS_Miss:delay:0.000277778 IN P_TS_Inspc:1 OUT
T_MS_Find:uniform:0.000555556  IN P_MS_Inspc:1 OUT P_MS_Repair:1
T_MS_Miss:delay:0.000277778 IN P_MS_Inspc:1 OUT
T_ES_Miss:delay:0.000277778 IN P_ES_Inspc:1 OUT
T_ES_Find:uniform:0.000555556  IN P_ES_Inspc:1 OUT P_ES_Repair:1
T_CF_Find:uniform:0.000555556  IN P_CF_Inspc:1 OUT P_CF_Repair:1
T_CF_Miss:delay:0.000277778 IN P_CF_Inspc:1 OUT
T_WI_Find:uniform:0.000555556  IN P_WI_Inspc:1 OUT P_WI_Repair:1
T_WI_Miss:delay:0.000277778 IN P_WI_Inspc:1 OUT
T_Alarm_Inspc:delay:0.0003 IN P_Alarm_Inspc:1 P_Inspection_Inactive:1
    ↪ OUT P_Inspection:1
T_ES_Repair:lognorm:1.66676:0.5 IN P_ES_Crew:1 P_Heat_Generation:1 OUT
    ↪  P_Crew:1 RESET P_External_State:P_External_Short:P_ES_lock:
    ↪ P_ESA_lock
T_CF_Repair:lognorm:1.66676:0.5 IN P_CF_Crew:1 OUT P_Crew:1
    ↪ P_CFH_Repair:1 RESET P_Coolant:P_Coolant_Fault:P_CF_lock:
    ↪ P_CFA_lock
T_WI_Repair:lognorm:1.66676:0.5 IN P_WI_Crew:1 P_Heat_Generation:1 OUT
    ↪  P_Crew:1 RESET P_Hull_Integrity:P_Water_Ingress:P_WI_lock:
    ↪ P_WIA_lock
T_Collision_Over:instant IN P_MS_lock:1 P_TS_lock:1 P_BMS_lock:1
    ↪ P_EL_lock:1 P_IS_lock:1 P_ES_lock:1 P_CF_lock:1 P_WI_lock:1 OUT
    ↪ P_Obstacles:1
T_Emergency_Action:instant IN P_Thermal_Runaway:1 OUT
    ↪ P_Emergency_Action:1 P_Thermal_Runaway:1 MAX 1
T_Operational_Period:delay:87660 IN P_Operating:1 OUT
    ↪ P_Operation_Complete:1 MAX 1
T_ES_Crew:instant IN P_ES_Repair:1 P_Crew:1 OUT P_ES_Crew:1
T_CF_Crew:instant IN P_CF_Repair:1 P_Crew:1 OUT P_CF_Crew:1
T_WI_Crew:instant IN P_WI_Repair:1 P_Crew:1 OUT P_WI_Crew:1
T_Inspc_Progress:delay:0 IN P_Inspection:1 OUT P_Inspc_Progress:1
T_HA_Reset:instant IN P_HA_lock:1 P_Heat_Generation:1:inh OUT
```

```
    T_CF_Heat:delay:6 IN P_Coolant_Fault:1 P_CFH_lock:1:inh OUT
       ↪ P_Coolant_Fault:1 P_Heat_Generation:1 P_CFH_lock:1
    T_CFH_Repair:instant IN P_Heat_Generation:1 P_CFH_Repair:1 P_CFH_lock
       ↪ :1 OUT
    T_CFH_NR:delay:0 IN P_CFH_Repair:1 OUT

145 # End
```

Appendix C Uncertainty Quantification

The precision of the results presented in this work is quantified by estimates of the standard error. For a sample, s, with mean, $\bar{s}$, median, $\tilde{s}$, standard deviation, σ_s, approximated as normally distributed, their standard errors, respectively $\sigma_{\bar{s}}$ [37] and $\sigma_{\tilde{s}}$, are

$$\sigma_{\bar{s}} = \frac{\sigma_s}{\sqrt{n}} \quad \text{and} \quad \sigma_{\tilde{s}} = \sqrt{\frac{\pi}{2n}}\,\sigma_s, \tag{A.12}$$

given a sample of size, n. For the p^{th} percentile, P_p, of the sample, $\sigma_{\tilde{s}}$ is a special case (*i.e.* P_{50}) of its standard error [38], σ_{s_p}, given by

$$\sigma_{s_p} = \frac{\sigma_s}{\sqrt{n}} \frac{\sqrt{p - p^2}}{\phi(z_p)}, \tag{A.13}$$

being dependent on the probability density of a standard normal distribution [39], $\phi(\cdot)$, at z_p, such that

$$\phi(z_p) = \frac{1}{\sqrt{2\pi}} \exp\left(-\frac{z_p^2}{2}\right), \tag{A.14}$$

where z_p is the value of the standard-normal quantile function [40] at the given percentile, p, given by

$$z_p = \sqrt{2}\,\operatorname{erf}^{-1}(2p - 1), \tag{A.15}$$

with $\operatorname{erf}(\cdot)$ being the error function [40], defined as

$$\operatorname{erf}(\zeta) = \frac{2}{\sqrt{\pi}} \int_0^{\zeta} e^{-\xi^2}\, \mathrm{d}\xi. \tag{A.16}$$

For values representing a probability or a proportion of a sample, $\mathbb{P}$, the standard error, $\sigma_{s_{\mathbb{P}}}$ [41], is given by

$$\sigma_{s_{\mathbb{P}}} = \sqrt{\frac{\mathbb{P} - \mathbb{P}^2}{n}}. \tag{A.17}$$

If a value s_Σ is produced by the summation of independent quantities, s_0, s_1, s_2, …, s_{n-1}, then its standard error, σ_{s_Σ} [37], is a function of the uncertainties of its summands, *i.e.* σ_{s_0}, σ_{s_1}, σ_{s_2}, …, $\sigma_{s_{n-1}}$, such that

$$\sigma_{s_\Sigma} = \sqrt{\sum_{i=0}^{n-1} \sigma_{s_i}^2}. \tag{A.18}$$